https://doi.org/10.1016/j.jsv.2017.04.042

On the sound insulation of acoustic metasurface using a sub-structuring approach

Xiang Yu,[1)] Zhenbo Lu,[2)] Li Cheng,[3)] and Fangsen Cui[1)*]

1) Institute of High Performance Computing, A*STAR, Singapore 138632

2) Temasek Laboratories, National University of Singapore, Singapore, 117411

3) Department of Mechanical Engineering, The Hong Kong Polytechnic University, Hong Kong 999077

*cuifs@ihpc.a-star.edu.sg

Abstract

The feasibility of using an acoustic metasurface (AMS) with acoustic stop-band property to realize sound insulation with ventilation function is investigated. An efficient numerical approach is proposed to evaluate its sound insulation performance. The AMS is excited by a reverberant sound source and the standardized sound reduction index (SRI) is numerically investigated. To facilitate the modeling, the coupling between the AMS and the adjacent acoustic fields is formulated using a sub-structuring approach. A modal based formulation is applied to both the source and receiving room, enabling an efficient calculation in the frequency range from 125 Hz to 2000 Hz. The sound pressures and the velocities at the interface are matched by using a transfer function relation based on “patches”. For illustration purposes, numerical examples are investigated using the proposed approach. The unit cell constituting the AMS is constructed in the shape of a thin acoustic chamber with tailored inner structures, whose stop-band property is numerically analyzed and experimentally demonstrated. The AMS is shown to provide effective sound insulation of over 30 dB in the stop-band frequencies from 600 to 1600 Hz. It is also shown that the proposed approach has the potential to be applied to a broad range of AMS studies and optimization problems.

Keywords: acoustic metasurface, sound insulation, sound reduction index, ventilation.

1. Introduction

Sound insulating structures are widely used in various engineering and architectural applications. Structures such as a heavy wall can achieve high sound insulation. When ventilation or heat conduction is necessary, however, introducing an opening can significantly deteriorate the overall sound insulation performance of the structure. The sound insulation property of a structure is usually adversely dominated by the poor performance of the opening, making it difficult to conciliate noise reduction and ventilation at the same time. Previous studies have considered the use of porous material [1] and partially open double glazing [2] to treat the opening, but the sound reduction that can be achieved is still marginal.

In recent years, acoustic metamaterials (AMM) received much attention and appeared to open up a new direction for designing acoustic devices, exemplified by research in the field of sonic crystals [3], AMM with negative effective mass [4], negative effective bulk modulus [5] and double-negative AMM [6]. The existing AMMs are often realized either by resonant systems such as Helmholtz resonators (or elastic membranes with attached mass), or by periodic lattices based on the Bragg scattering. Focusing on the ventilation applications, several researchers have demonstrated the existence of acoustic stop-bands in acoustic ducts lined with periodic scatters [5-7]. The forming of the acoustic stop-band is related to both the individual property of the scatterer and the periodicity. However, the acoustic duct systems presented in these studies are very bulky, which hampers their applicability in real-world applications.

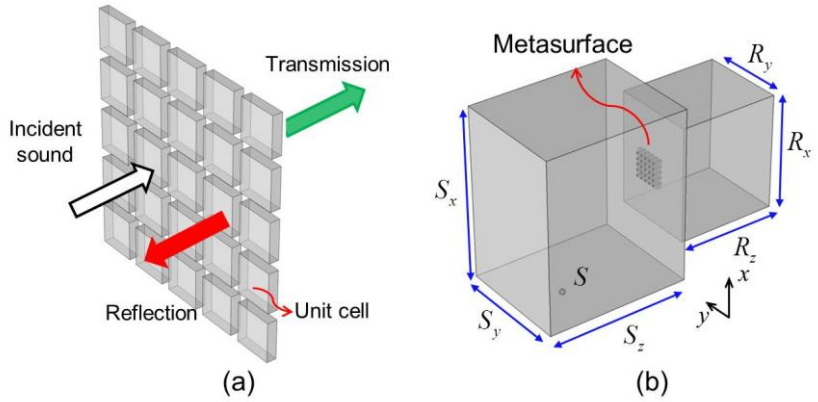

Fig. 1. (a) AMS constructed of structured unit cells for controlling and manipulating sound waves; (b) AMS connecting a sound source field and a receiving room.

The use of AMM for practical noise control is more desirable with compact size and broadband performance. With an emphasis on the sub-wavelength property, the realization of acoustic metasurface (AMS) may overcome some of these limitations. As illustrated in Fig. 1(a), an AMS is constructed by stacking structured unit cells in a periodic pattern as a planar array, aiming to realize a certain acoustic function such as high reflection, high absorption or negative refraction. Recent studies reported the design of AMS based on Helmholtz resonators, locally resonant absorbers and artificial Mie resonances [8-10]. The objective of the present study is to use the concept of AMS to realize a surface structure for broadband sound insulation while allowing for air ventilation. To this end, the unit cell is constructed in the shape of a thin air chamber with apertures on the front and rear surfaces (see Fig. 9 below). The structure inside the air chamber is tailored by adding partitions, ideally forming an acoustic stop-band, to prevent noise transmission. The proposed structure is applicable to those working environments where noise mitigation, ventilation and heat

conduction are simultaneously required. Typical examples are ventilation windows with high noise insulation, sound enclosures for engine and machinery equipment, etc.

Most of the existing analyses on AMS carried out to date were focusing on the structural dispersion curves based on eigen-state properties [8, 9]. As an equivalent acoustic medium, the effective material properties of the AMS can be deducted from the analyses based on small-scale samples under normal incidence condition. However, when using AMS in real applications, its acoustic response is not only determined by its eigen properties, but also by the characteristics of the coupled acoustic fields. For example, the size, arrangement of the AMS, and most importantly, the sound incidence pattern can all affect the results, which makes the so-called "*in-situ* performance" significantly different from the *theory* [11]. As our target is to design AMS for sound insulation, a representative configuration in Fig. 1(b) is considered, where the AMS is connecting a sound source room and a receiving room. Such a configuration is described in ISO 10140 [12] for guiding a standardized SRI measurement, provided that certain acoustic conditions for the two rooms are satisfied. Since the two rooms are three-dimensional (3D), and the acoustic excitation and radiation are not limited to a particular angle, the resultant acoustic performance is inherently different from the normal incidence case. This study addresses the SRI prediction based on the standardized configuration as illustrated in Fig. 1(b).

Numerical models are useful tools to understand the physical phenomena and tune the acoustic performance. Finite element method (FEM) has been applied to model AMS composed of both acoustical (e.g. Helmholtz resonator) and structural

(e.g. membrane with/without attached mass) elements [8-10]. Eigen-state analyses and effective material parameter retrieval based on small scale samples have been demonstrated. However, it is definitely challenging to extend those FEM models for predicting the SRI, mainly hampered by the extremely heavy computational cost. The FEM requires a convergence criterion of at least six to eight nodes per wavelength. To predict the SRI at 2000 Hz, for example, the element size should be smaller than 0.03 m (wavelength in air is 0.18 m), which means that millions of elements are needed to represent a 3D room with side length in the meter range. This greatly restricts the applicability of FEM for such kind of problems.

To evaluate the acoustic performance of the AMS and tackle the numerical difficulties, this study presents a sub-structuring approach with hybrid theoretical-numerical techniques to evaluate the SRI under laboratory test setting. The sub-structuring approach first characterizes the acoustic properties of the two rooms separately, and then couples the AMS to solve the overall response. The simple room geometry allows analytical treatment to expedite the calculation, whilst the complex AMS can still be modeled by detailed methods without encumbering the total calculation process. Similar hybrid modeling has been demonstrated [13], with the continuity condition at the interface being written in a modal integration form. However, to describe the AMS by modal matching is mathematically tedious. A more convenient matching technique is developed here by writing the coupling at the averaged *patches, i.e.*, a small surface element segmented over the AMS, within which the acoustic properties are assumed as uniform. Depending on the sound

transmission characteristics, two types of AMS are considered in the formulation. One type can be described by effective material properties, which treats the AMS as an equivalent acoustic medium. The other type has separated unit cells, which means that sound can only pass through the normal surface of each cell without propagating within the surface. Such an AMS is treated as a cluster of acoustic elements, and the transfer matrix of each unit cell is utilized to connect the acoustic fields in the two rooms. Since the unit cells are structured in irregular shapes, FEM remains the most suitable tool to model their properties. The analytical room modeling, interface matching and AMS modeling constituting the whole numerical framework are discussed in Sec. 2.

For illustration purposes, several numerical examples are investigated in Sec. 3. Both the proposed sub-structuring approach and the conventional FEM are employed to predict the SRI, where the FEM results within the convergence limit are used to validate the proposed approach. To realize an AMS for both sound insulation and ventilation, the unit cell in the shape of an opened air chamber with a tailored inner structure is constructed. Experiments were conducted to confirm the acoustic property of the unit cell, showing stop-band behavior from 600 Hz to 1600 Hz. The SRI of the proposed AMS is then numerically predicted using the proposed approach, with comparisons with other unit cell configurations.

2. Formulation of the sub-structuring approach

2.1 Source and receiving room modeling

Let us consider an AMS connecting a reverberant source room and a receiving room as shown in Fig. 1(b). The AMS is composed of structured unit cells aiming at blocking the noise transmission in a specific frequency range. This section presents a theoretical framework for SRI prediction under the laboratory setting as specified in ISO 10140 [12]. To generate a diffuse sound source, the rectangular room has rigid wall surfaces and is excited by a point sound source *S*. The size of the source room is $S_x \times S_y \times S_z$, and that of the receiving room is $R_x \times R_y \times R_z$. The sound pressure fields inside the rectangular room can be analytically decomposed into the rigid-walled acoustic modes as:

$$P_r(x,y,z) = \sum_m a_r^m \varphi_r^m(x,y,z) = \sum_m a_r^m \cos(k_x x)\cos(k_y y)\cos(k_z z) \ , \tag{1}$$

where P_r is the sound pressure; a_r^m and φ_r^m the amplitude and mode shape function of the eigenmodes; m denotes the modal number; k_x, k_y and k_z are the wavenumbers: $k_x = m_x\pi / S_x$, $k_y = m_y\pi / S_y$ and $k_z = m_z\pi / S_z$; m_x, m_y and m_z are modal numbers: $m_x, m_y, m_z = 0,1,2\cdots$, in the *x*-, *y*- and *z*- directions, respectively. The same modal expansion applies to the receiving room.

The sound pressure generated by the point source is transmitted into the receiving room by the AMS. Inside the two rooms, the general formulation of the pressure field in the presence of point source and acoustic boundary has been well-documented [14].

By incorporating Helmholtz's wave equation into a Green's formulation, the acoustic response solely due to the point source is:

$$a_r^m N_r^m (k^2 - k_m^2) = \int_{V_r} q\varphi_r^m \delta(x_s, y_s, z_s) dV_r = q\cos(k_x x_s)\cos(k_y y_s)\cos(k_z y_z) \qquad (2)$$

where $k = \omega / c_0 = 2\pi f / c_0$, f is the excitation frequency, $c_0 = 343$ m/s is the sound speed in air. The air damping can be included in a complex sound speed as $c_0^* = c_0\sqrt{1 + j\eta_0}$, with η_0 being the damping loss factor.

$k_m = \sqrt{k_x^2 + k_y^2 + k_z^2} = 2\pi f_m / c_0$, f_m is the eigenfrequency of the room. V_r describes the air volume enclosed by the room. q is the strength of the point source, δ is the Dirac delta and coordinate (x_s, y_s, z_s) specifies location of the sound source. The modal mass N_r^m is

$$N_r^m = \int_{V_c} \varphi_r^m \varphi_r^m dV_c = \int_0^{S_x}\int_0^{S_y}\int_0^{S_z} \cos^2(k_x x)\cos^2(k_y y)\cos^2(k_z z) dx dy dz\,, \qquad (3)$$

where

$$\int_0^{S_x} \cos^2(k_x x) dx = \begin{cases} S_x, & m_x = 0 \\ 0.5S_x, & m_x \neq 0 \end{cases},$$

and the same expressions apply to the *y*- and *z*- directions. In the calculation, the series need to be truncated leading to a finite number of eigenmodes to be used. To ensure the convergence, the number of modes N_m is truncated until the eigenfrequency f_m exceeds twice of the maximum calculation frequency.

It is assumed that sound can only pass through the AMS and all the other room walls are rigid. In that case the AMS can be considered as a vibrating boundary whose

normal velocity is V_n, and the coupling with the acoustic cavity can be written as [14, 15]:

$$a_r^m N_r^m (k^2 - k_m^2) = \int_{S_r} -(\partial P_r / \partial n)\varphi_r^m dS_r = \int_{S_r} j\rho_0 \omega V_n \varphi_r^m dS_r \quad , \tag{4}$$

where S_r is the surface area of the AMS, *n* denotes the direction normal to the surface. $\partial P_r / \partial n = -j\rho_0 \omega V_n$, ρ_0 is the air density, taken as $\rho_0 = 1.25$ kg/m^3. The above equation is commonly used as the governing equation for modeling sound transmission through partitions, such as flexible plate [16], wall with slit or opening [13], porous material [17], etc. If the partition structure is simple, analytical modeling can be applied and standard modal matching at the connecting interface can be used to get the system response. However, the AMS are usually designed in complex structures. Using modal matching is mathematically tedious and thus becomes not very practical.

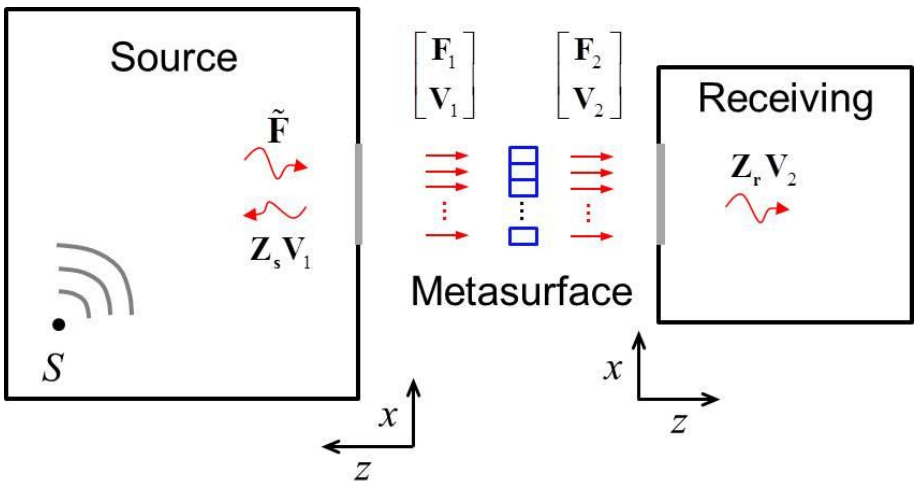

Fig. 2. Sub-structuring approach for modeling the sound transmission between two rooms through the AMS.

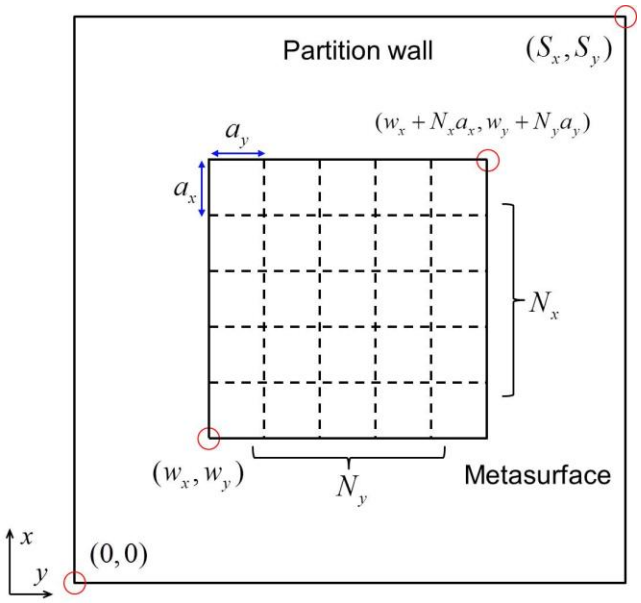

Fig. 3. Modeling of the AMS mounted on the common partition wall.

Here, a sub-structuring approach is proposed to facilitate the modeling. Figure 2 illustrates the system which is divided into a source room, a receiving room and the AMS in the middle. The AMS is excited by initial force $\tilde{\mathbf{F}}$ due to the point source, and coupled to the two rooms through acoustic impedances $\mathbf{Z}_s$ and $\mathbf{Z}_r$ .The AMS, as depicted in Fig. 3, is composed of N_x by N_y unit cells of side length $a_x \times a_y$. The origin of the Cartesian coordinate system coincides with the room corner, and the lower left and upper right corners of the AMS are located at (w_x, w_y) and (w_x+$N_x a_x$, w_y+$N_y a_y$), respectively. Let us denote the surface area of each unit cell by a small "patch", which connects the acoustic fields on its both sides either acoustically or structurally. If the patch size is smaller than half of a wavelength in the acoustic domain, it is reasonable to consider its vibroacoustic response in an averaged sense, enabling an averaged pressure and velocity to describe each patch [18]. The force $\tilde{\mathbf{F}}$ is a vector containing the same number of elements as the patch numbers $N_x \times N_y$, and the two impedances

$\mathbf{Z}_{\mathbf{s}}$ and $\mathbf{Z}_{\mathbf{r}}$ are square matrices of order $N_x \times N_y$. For a patch located in row n_x and column n_y ($n_x = 1,2,\cdots N_x, n_y = 1,2,\cdots N_y$), the corresponding excitation force $\tilde{F}$ element averaged over its surface, which is obtained *a priori* to the coupling, has:

$$\tilde{F} = \int P_r dS = \int \sum_m a_r^m \varphi_r^m dS \ , \tag{5}$$

where the expression of a_r^m can be found in Eq. (2), leading to

$$\tilde{F} = \sum_m \frac{Q\int \varphi_r^m dS}{N_r^m (k^2 - k_m^2)} = \sum_m \frac{Q}{N_r^m (k^2 - k_m^2)} \int_{w_x+(n_x-1)a_x}^{w_x+n_x a_x} \int_{w_y+(n_y-1)a_y}^{w_y+n_y a_y} \cos(k_x x)\cos(k_y y) dxdy \ , \tag{6}$$

where the source term Q is defined as $Q = q\cos(k_x x_s)\cos(k_y y_s)\cos(k_z y_z)$. The integration of the mode shape function in the *x*- direction is:

$$\int_{w_x+(n_x-1)a_x}^{w_x+n_x a_x} \cos(k_x x) dx = \begin{cases} w_x + n_x a_x - [w_x + (n_x - 1)a_x] = a_x, & k_x = 0 \\ \{\sin[k_x(w_x + n_x a_x)] - \sin[k_x(w_x + (n_x - 1)a_x)]\}/k_x, & k_x \neq 0 \end{cases}.$$

Similar expression can be obtained for the *y*- direction. The excitation forces $\tilde{F}$ for each patch are combined as the excitation force vector $\tilde{\mathbf{F}}$.

The coupling impedance between the AMS and the adjacent acoustic domain is derived from Eq. (4). Consider the sound pressure in the room excited by a patch "*a*" (in row n_x and column n_y) with an input velocity, resulting in a force at a receiving patch "*b*" (in row n_x' column n_y'). The acoustic impedance, or the transfer function between the input velocity and output force writes:

$$Z_{a,b} = F_b / V_a = \int P_r dS_b / V_a = \sum_m (a_r^m / V_a) \int \varphi_r^m dS_b \quad , \tag{7}$$

where V_a is the averaged velocity of patch *a* and F_b is the resulted force at patch *b*. Incorporating the expression of a_r^m obtained from Eq. (4) further leads to:

$$Z_{a,b} = \sum_m \frac{j\rho_0\omega}{N_r^m (k^2 - k_m^2)} \int_{S_a} \varphi_r^m dS_a \int_{S_b} \varphi_r^m dS_b \quad , \tag{8}$$

where $\int_{S_a} \varphi_r^m dS_a = \int_{w_x+(n_x-1)a_x}^{w_x+n_x a_x} \int_{w_y+(n_y-1)a_y}^{w_y+n_y a_y} \cos(k_x x)\cos(k_y y)dxdy$ and

$\int_{S_b} \varphi_r^m dS_b = \int_{w_x+(n'_x-1)a_x}^{w_x+n'_x a_x} \int_{w_y+(n'_y-1)a_y}^{w_y+n'_y a_y} \cos(k_x x)\cos(k_y y)dxdy$, respectively.

It is worth noting that the initial excitation force $\tilde{\mathbf{F}}$ and the acoustic impedances $\mathbf{Z_s}$ and $\mathbf{Z_r}$ are calculated before the AMS is coupled together. The vibroacoustic coupling at the interface facing towards the source room and the receiving room is written as:

$$\begin{aligned} \tilde{\mathbf{F}} &= \mathbf{Z_s V_1} + \mathbf{F_1} \\ \mathbf{F_2} &= \mathbf{Z_r V_2} \end{aligned} \quad , \tag{9}$$

where $\mathbf{V_1}$ and $\mathbf{V}_2$ are the velocity vectors of the AMS on both sides. $\mathbf{F_1}$ and $\mathbf{F_2}$ are the force vectors, describing the coupling through the AMS.

2.2 Acoustic metasurface modeling

As for the AMS modeling, two types of treatment are developed depending on the sound transmission characteristics through the AMS. The first treatment is for those AMS which can be considered as an equivalent acoustic material, such as sonic crystal constructed from elastic material with dynamic inclusions [3, 19]. The effective material properties, namely the complex mass density ρ_m and complex sound speed c_m , can be retrieved based on the available method [20]. As an equivalent fluid domain, the patches divided over the front and back surfaces of the

AMS are interconnected, as illustrated in Fig. 4(a). The coupling within the AMS can be written as:

$$\begin{bmatrix} \mathbf{F}_1 \\ \mathbf{F}_2 \end{bmatrix} = \begin{bmatrix} \mathbf{Z}_{11} & \mathbf{Z}_{12} \\ \mathbf{Z}_{21} & \mathbf{Z}_{22} \end{bmatrix} \begin{bmatrix} \mathbf{V}_1 \\ \mathbf{V}_2 \end{bmatrix}, \tag{10}$$

where $\mathbf{Z}_{11}$ and $\mathbf{Z}_{22}$ describe the coupling impedance between the patches on the same surface, $\mathbf{Z}_{12}$ and $\mathbf{Z}_{21}$ describe the transfer impedance between the two surfaces. The four impedances are square matrices of order $N_x \times N_y$, and their element expressions can be found similar to Eq. (8), simply by changing air ρ_0 and c_0 to the effective ρ_m and c_m of the AMS.

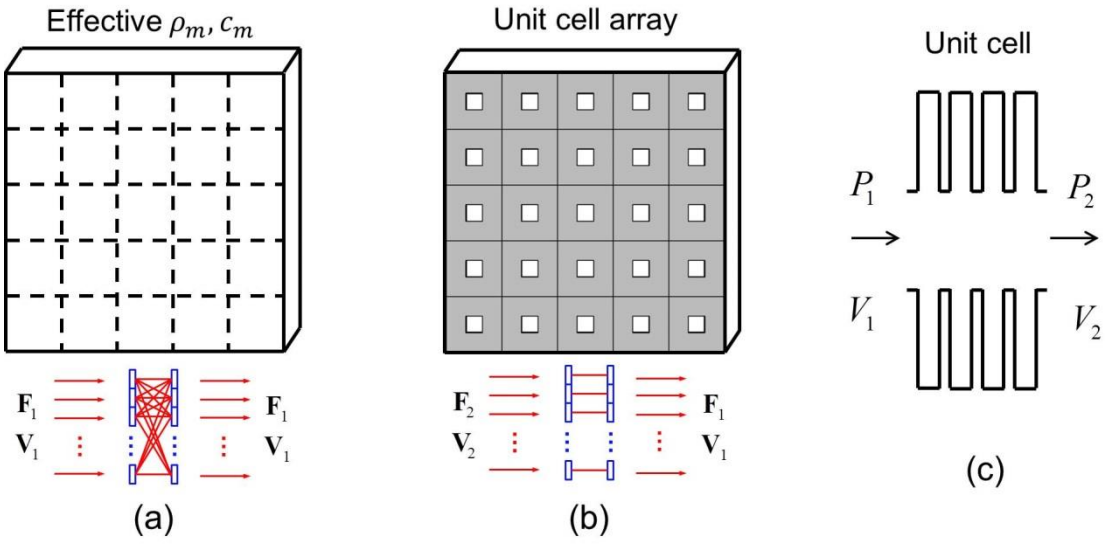

Fig. 4. AMS modeled as: (a) an equivalent acoustic domain; (b) an array of acoustic elements. (c) AMS with unit cells designed in an air duct with periodic resonators.

The second treatment is developed for AMS which is composed of separate unit cells, as shown in Fig. 4(b). The sound wave is assumed to be transmitted only through each cell in the normal direction, without being able to propagate within the

surface direction. Such a configuration can be used to describe AMS with decorated membrane resonators [9], and AMM with local resonant membranes [21-23], whose resonant component is constraint over a relatively rigid frame. Given a sound incidence, each unit cell is assumed to be acoustically locally reacting, such that the dynamic equilibrium condition can be established at each unit cell.

Aiming to realize an AMS for sound insulation and ventilation, the unit cell in the shape of a thin air chamber with apertures on the front and rear surfaces is constructed. The inner structure is tailored into multi-chambers to create local resonances, aiming to form an acoustic stop-band. The cross-section of a unit cell is illustrated in Fig. 4(c), which can be considered as a waveguide attached with periodic scatterers. The theoretical wave propagation and the existence of stop-band in such waveguide have been studied [7, 24-26]. In this investigation, a number of unit cells are stacked up in a planar array, turning in to the configuration in Fig. 4(b).

To model each unit cell, the sound transmission through the duct can be treated by the well-known transfer matrix method. The duct inlet is connected to the source room and the outlet is connected to the receiving room. Assuming the cut-off frequency of the duct inlet is higher than the frequency of interest, the four-pole parameters can be used to describe the inlet-outlet relationship:

$$\begin{bmatrix} F_1 \\ V_1 \end{bmatrix} = \begin{bmatrix} A & B \\ C & D \end{bmatrix} \begin{bmatrix} F_2 \\ V_2 \end{bmatrix}, \tag{11}$$

where *A*, *B*, *C* and *D* are the four-pole parameter of a unit cell. F_1 and F_2, V_1 and V_2 are the force and velocity at the inlet and outlet, respectively. The four-pole parameters for each unit cell can be obtained by:

$$\begin{aligned} A = P_1 / P_2, C = V_1 / P_2 S_o, \ \text{when} \ V_2 = 0 \\ B = P_1 S_o / V_2, D = V_1 / V_2, \ \text{when} \ P_2 = 0 \end{aligned}, \tag{12}$$

where S_o is the surface area of the opening. The above relation can be deducted from analytical method if the duct structure is simple [27, 28], or solved from numerical methods by using FEM or BEM [29, 30]. For the periodic scatterers, many scatterer types can be considered by the proposed technique, such as Helmholtz resonator [31], side-branch scatterer or quarter-wave tube [7, 24, 25].

Then, by combining Eq.(11) with Eq. (9), the equations for describing the coupled systems yield:

$$\begin{bmatrix} \mathbf{I} & \mathbf{0} & \mathbf{Z_s} & \mathbf{0} \\ \mathbf{-I} & \mathbf{A} & \mathbf{0} & \mathbf{B} \\ \mathbf{0} & \mathbf{C} & \mathbf{-I} & \mathbf{D} \\ \mathbf{0} & \mathbf{I} & \mathbf{0} & \mathbf{-Z_r} \end{bmatrix} \begin{bmatrix} \mathbf{F_1} \\ \mathbf{F_2} \\ \mathbf{V_1} \\ \mathbf{V_2} \end{bmatrix} = \begin{bmatrix} \tilde{\mathbf{F}} \\ \mathbf{0} \\ \mathbf{0} \\ \mathbf{0} \end{bmatrix}. \tag{13}$$

The velocity response of the AMS, $\mathbf{V_1}$ and $\mathbf{V_2}$ on its both sides, can be solved from the Eq. (13).

2.3 SRI calculation

To evaluate the sound insulation, the responses inside the two rooms are further determined. The sound field inside the receiving room is entirely due to the vibrating boundary $\mathbf{V_2}$. From Eq. (4), one as:

$$a_{r_2}^m = \frac{j\rho_0\omega}{N_{r_2}^m(k^2-k_m^2)}\int V_2\varphi_{r_2}^m dS \ . \tag{14}$$

where r_2 stands for the receiving room. For the source room r_1 , the response is a linear summation of the initial excitation due to the point source and the coupling due to the vibrating boundary $\mathbf{V_1}$,

$$a_{r_1}^m = \frac{1}{N_{r_1}^m(k^2-k_m^2)}(Q + j\rho_0\omega\int V_1\varphi_{r_1}^m dS) \ . \tag{15}$$

The modal amplitude expressions are used to calculate the sound pressure at any point inside the room. The Sound Pressure Level (SPL) is given by:

$$L_r = 10\log(P_{rms}^2 / P_0^2) = 10\log(|\sum_m (a_r^m\varphi_r^m)^2| / 2P_0^2) \ , \tag{16}$$

where P_{rms} is the *root-mean-square* sound pressure, $P_{rms} = P_r / \sqrt{2}$ for time-harmonic analysis. P_0 is the reference sound pressure, taken as $P_0 = 20\ \mu$Pa in air.

The spatial averaged SPL $\overline{L_r}$ is:

$$\overline{L_r} = \int_{V_r} L_r dV_r / V_r = 10\log(\sum_m \left|a_r^m\right|^2 N_r^m / 2V_r P_0^2) \ , \tag{17}$$

where $V_r = S_x S_y S_z$ for the source room and $V_r = R_x R_y R_z$ for the receiving room. The level deference *D* between the source and receiving room is $\overline{L_{r1}} - \overline{L_{r2}}$, and the SRI for specifying the sound insulation performance is calculated as [12]:

$$SRI = \overline{L_{r1}} - \overline{L_{r2}} + 10\log(S / S_\alpha) \tag{18}$$

where S_r is the total area of the AMS, S_α is the equivalent sound absorption area of the receiving room, $S_\alpha = 0.16V_r / RT$ with *RT* being the reverberation time.

2.4 Source room diffuseness

To generate a diffuse sound source, a rectangular room with side lengths of 6m×4m×5m in the *x*-, *y*- and *z*- directions is used to excite the AMS as shown in Fig. 5. The total volume V_{r1} =120 m^3 satisfies the recommendation in ISO 10140, and the side lengths have at least 10% difference. The diffuseness is verified before using it for SRI prediction.

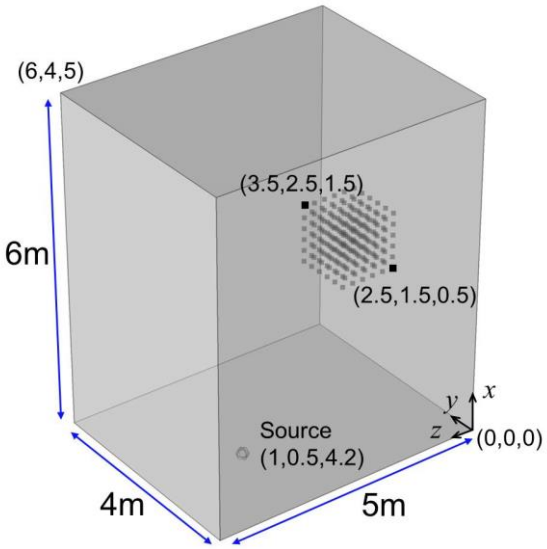

Fig. 5. A representative source room to excite the test AMS structure.

Theoretically, the diffuse condition is more likely to occur with sufficient number of room modes. The number of normal modes up to a frequency *f* can be accurately determined from Eq. (3), or approximately estimated by:

$$N_m \approx \frac{4\pi}{3} V_r \left(\frac{f}{c_0}\right)^3 + \frac{\pi}{4} S_r \left(\frac{f}{c_0}\right)^2 + \frac{L}{8}\frac{f}{c_0} \ . \tag{19}$$

For the present source room dimension, $V_r = 120\ \mathrm{m}^3$, the total area of room boundary $S_r = 148\ \mathrm{m}^2$, and the sum of side lengths $L = 60\ \mathrm{m}$. In Table 1, the number of the acoustic modes N_m within the frequency range from 0 to the upper limit of each 1/3 octave band are tabulated. The *frequency* from 63 Hz to 2000 Hz refers to the center frequency of each band. Previous work by Papadopoulos [32], Nelisse and Nicolas [33] suggested the diffuse condition could be met if 20-30 normal modes exist per bandwidth. This corresponds to 125 Hz in Table 1. In addition to the room modes, the spatial uniformity of sound pressure field is further checked. The standard deviation of SPL for a number of points sampled in the source room is calculated [2],

$$SD = \sqrt{\sum_{1}^{N_r} (L_r - \overline{L_r})^2 / N_r} \tag{20}$$

where L_r is the SPL at the sampling points, calculated via Eq.(16), $\overline{L_r}$ is their averaged value, N_r is the total number of sampling points. As sketched in Fig. 5, the sampling region is selected from (2.5, 1.5, 0.5) m to (3.5, 2.5, 1.5) m, a cubic volume with a side-length of 1 m. The sampled points have equal spacing of 0.2 m between each other in the *x*-, *y*- and *z*- directions. The air damping is taken as $\eta_0 = 0.005$. Figure 6 shows the standard deviation of SPLs, which decreases with increasing frequency. Once the standard deviation stabilizes below 1.5 dB, roughly from 125 Hz to 2000 Hz, the source room is qualified as diffuse enough [32, 33].

Table 1. The number of acoustic modes N_m within the frequency range from 0 to the upper limit of each 1/3 octave band.

Frequency	N_m	Frequency	N_m	Frequency	N_m	Frequency	N_m
63 Hz	11	160 Hz	109	400 Hz	1347	1000 Hz	18759
80 Hz	19	200 Hz	197	500 Hz	2512	1250 Hz	37200
100 Hz	33	250 Hz	358	630 Hz	5055	1600 Hz	73519
125 Hz	58	315 Hz	695	800 Hz	9891	2000 Hz	145760

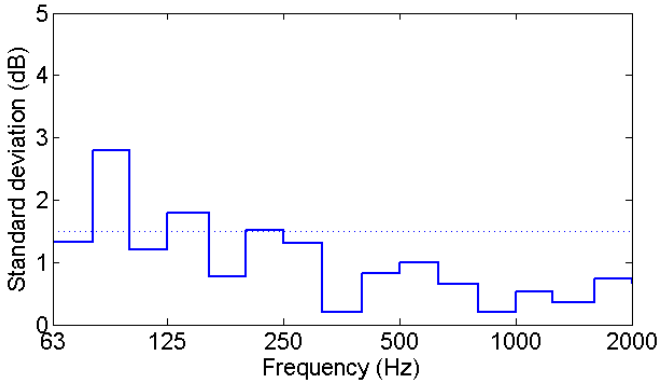

Fig. 6. Standard deviation of SPLs in the sampled region in the source room.

Another important observation here is an indication of the required computational cost. Table I shows that, to cover a medium high frequency range, the number of room modes to be included is very large. If 3D FEM analysis is conducted, the element size needs to be very small and the total number of degrees of freedom (n-DOF) is inevitably huge. This may cause tremendous troubles and nevertheless, it is not worth spending excessive computational resource on rooms, while the focus would be on AMS design and its optimization. The proposed approach can resolve the problem, by applying analytical modeling for the two rooms and packaging the coupling under a sub-structuring framework. In the low to mid-high frequency range from 125 Hz to

2000 Hz, the number of eigenmodes required for modeling the source room is still capped in the order of 10^6. The computational efficiency of the proposed approach and its advantage over traditional FEM analysis will be discussed in the specific numerical examples.

3. Numerical examples

This section presents validation of the proposed approach and investigations on a few numerical examples. In the following sub-sections, Sec. 3.1 demonstrates an air opening, as an example of the AMS which can be treated as an equivalent acoustic medium. Sec. 3.2 studies the AMS composed of separated unit cells. As sketched in Fig. 7, the source room as studied in Sec. 2.4 is used to generate the acoustic excitation, and a receiving room with a dimension of 3.5×4×3 m is used to measure the transmitted sound. A square-shaped opening (1×1 m) between two rooms is considered. The center of the opening is located at 3 m from the floor of the source room, and 2 m from the floor of the receiving room. In the following studies, the room and the opening dimensions are kept unchanged. The sub-structuring formulation as described in Sec. 2 is implemented in MATLAB code. The SPLs in the source and receiving rooms are calculated, and then the SRI of the structure considered at the opening is determined.

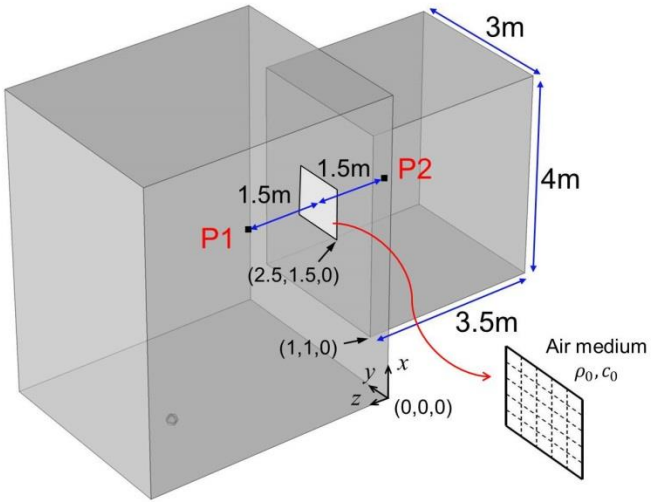

Fig. 7. Configuration and dimensions of the source room, reciving room and opening.

3.1 Treatment as equivalent acoustic medium

The first case considers a simple air opening as shown in Fig. 7. The objective is to validate the AMS treatment of the first type, i.e., as an equivalent acoustic medium. To model the air opening as a fluid domain, previous work by the authors has developed the necessary impedance expressions required by Eq. (10). The property of the air medium is given by ρ_0 and c_0 [15]. The idea is that if the approach works for the simplest air opening case, AMS of this type can be handled by changing air property to the effective AMS property. The air opening is divided into 10×10 patches, and the thickness of the opening is taken as 0.01 m. The SPL at two receiving points, located 1.5 m away from the center of the opening (P1 in the source room and P2 in the receiving room), are calculated in the linear frequency range from 10 Hz to 300 Hz. The frequency step-size is chosen as 1.5 Hz. A sufficient number of room modes have been included in the calculation.

To validate the theoretical approach, a FEM model is built using the Acoustic module in the commercial software COMSOL Multiphysics. The same room and sound source conditions are defined in the FEM model. The FEM mesh (free-tetrahedral element) is generated according to the acoustic wavelength at 200 Hz, where $\lambda = 343/200 = 1.7$ m. By using six-element description of one wavelength, the biggest element size is 0.28 m, and the total number of DOFs for the system is around 1.2×10^5. To solve the system response takes about 10 hours CPU time, performed on a workstation with 16-core CPU and 32 GB RAM. The SPLs at P1 and P2, calculated using the proposed approach and FEM, are presented and compared in Figs. 8 (a) and (b), respectively. It can be seen that the results from the proposed approach and FEM agree very well below 200 Hz, in the range where FEM is sufficiently reliable. Slight deviation starts to occur beyond 200 Hz, which exposes the limit of FEM model for coping with higher frequencies. This example shows the validity of the present treatment.

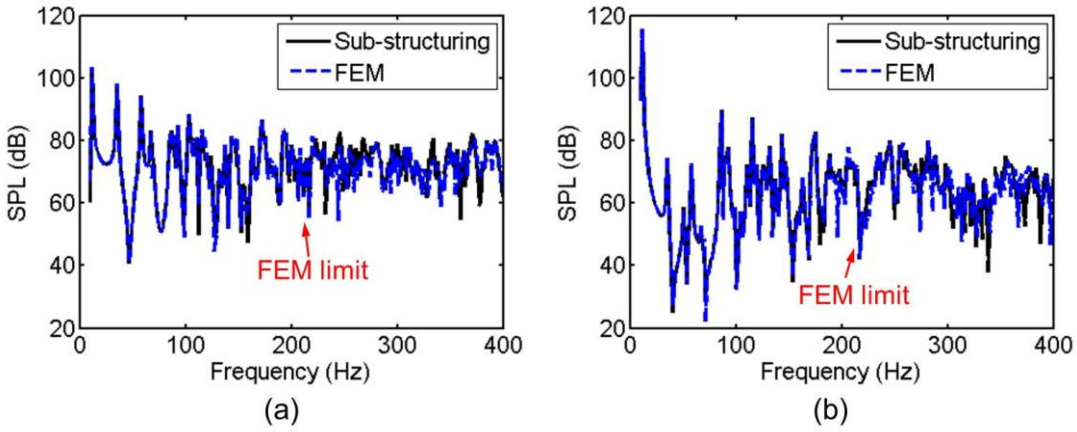

Fig. 8. Comparisons between the SPLs calculated using the proposed approach and FEM, at: (a) P1 in the source room and (b) P2 in the receiving room.

3.2 Treatment as separate acoustic elements

AMS composed of unit cells in the form of an acoustic waveguide with periodic scatterers is investigated. As shown in Fig. 9 (a), the structure to fit the test opening is divided into 5×5 unit cells, each with a cross-sectional area of 0.2×0.2 m. The unit cell is a rectangular air chamber, with aperture of 0.06×0.06 m at the center of the front and rear surface, as sketched in Fig. 9 (b). The air chamber is divided into several sub-chambers by adding internal partitions. The width of each sub-chamber is 0.02 m, and that of the rigid partitions is 0.005 m. The periodicity *d* is therefore 0.025 m. Due to the thickness limit, finite number of periodic sub-chambers is connected to produce the acoustic stopband effect. Connecting four sub-chambers gives a total thickness of around 0.1 m, and the two-dimensional (2D) cross-section of the unit cell is shown in Fig. 9(c).

The theoretical Bloch wave theory applied to the proposed structure is briefly analyzed. As a waveguide loaded with periodic scatters, Bradley [24, 25] first demonstrated the existence of Bragg stop-bands and scatterer resonance stop-bands, which leads to the later development of acoustic metamaterials [7, 26]. The Bloch dispersion relation points out that the Bragg stop-bands is likely to occur when the frequency and periodic resonators satisfy the following condition: $f = nc_0 / 2d, n = 1, 2, 3\cdots$. Given a periodicity of *d*=0.025 m, the first Bragg stop-band exceeds 6000 Hz, which is beyond the frequency range of interest here. The scatterer resonance stop-band occurs near the resonant frequency of the side-branch scatterer. The 2D configuration as shown in Fig. 9 (c) can be considered as a periodic

arrangement of quarter-wave tubes, whose resonant frequencies are $f = nc_0 / 4h_r$, $n = 1, 3 \cdots$. h_r is the height of the tube. h_r =0.07 m yields the first resonance at 1200 Hz. Note that the stop-band frequency range, namely the bandwidth, is affected by the width of the sub-chamber, dissipation loss, periodicity of the sub-chambers, etc.

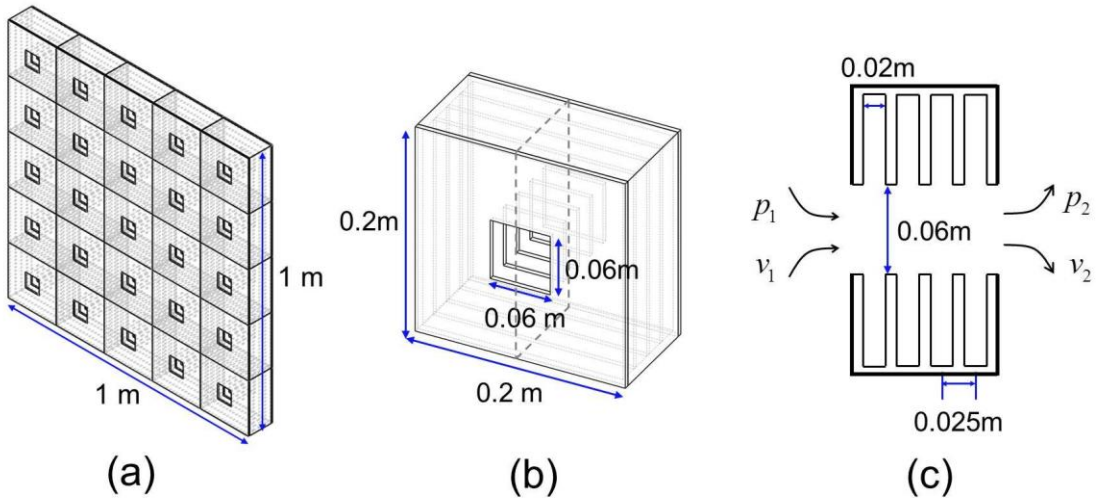

Fig. 9. (a) Acoustic metasurface constructed from a planar array (5×5) of unit cells; (b) 3D configuration of a unit cell, consisting of a serious of expansion chambers; (c) Inner dimension of the 2D cross-section.

To understand the acoustic property of the unit cell, both numerical and experimental analyses are conducted to study its sound transmission characteristics. A picture of the fabricated unit cell sample is shown in Fig. 10(a), which is made of transparent acrylic panels of 5 mm thickness. The acoustic property of the unit cell, including transmission and absorption coefficient, is experimentally tested using the well-established four microphone-two load method [28]. For numerical investigation, a FEM model is built as shown in Fig. 10(b), where a waveguide with the same cross-section as the unit cell is excited by a normal plane wave from one end and radiates freely to the other end. A section of the waveguide is replaced by one unit cell in the

middle. The *transmittance*, or the transmission coefficient of the unit cell is calculated as the ratio between the transmitted power to the incident sound power. Note that all the wall structures of the unit cell are assumed as rigid in the simulation. In Fig. 11(a), the predicted and experimental transmittance results are plotted, showing very good agreement. A bandgap structure from 600 Hz to 1600 Hz is obtained, which coincides with the scatter resonance stop-band as explained above. In Fig. 11(b), the Transmission Loss (TL) characteristics of the unit cell from FEM calculation and experiment are compared. The theoretical and experimental curve shows very similar trend, although some discrepancies are found at the TL peak region. A plausible explanation is that small percentage of sound leakage from the thin acrylic partitions is inevitable, making high TL (> 60 dB) very difficult to be achieved in experiment.

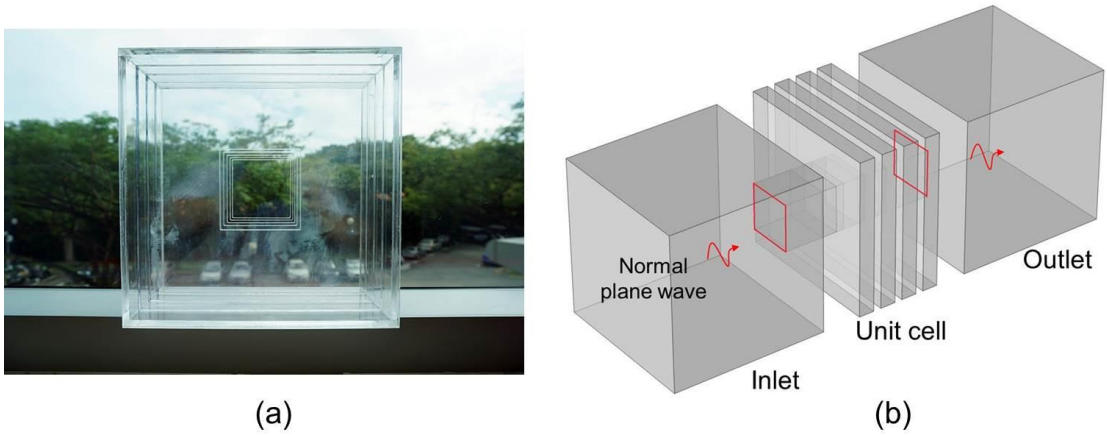

Fig. 10. (a) The fabricated unit cell sample for experimental test. (b) FEM model for calculating the transmission characteristics of a unit cell.

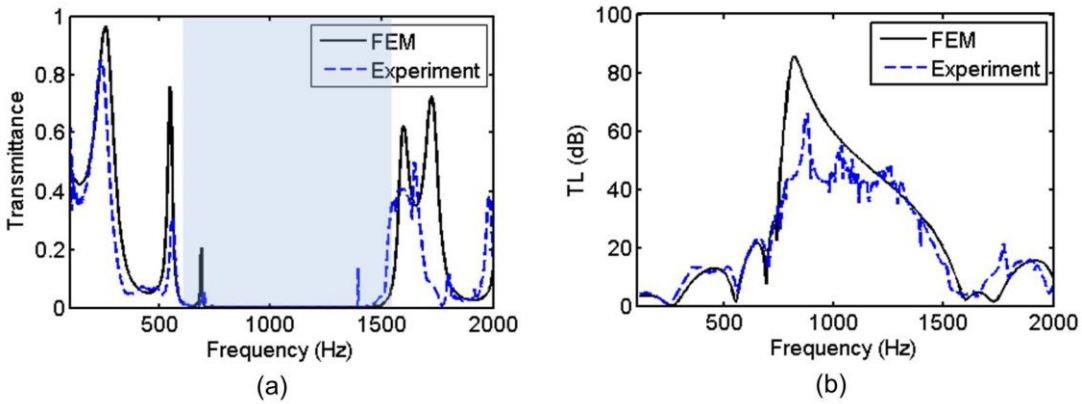

Fig. 11. (a) The transmittance versus frequency, the bandgap structure is marked in light blue. (b) Transmission loss of the unit cell.

Using the proposed approach, the SRI of the AMS in Fig. 9(a) is calculated from 125 Hz to 2000 Hz, and the result is presented in 1/3 octave bands. Within each band, 30 frequency points are logarithmically sampled and averaged. The four-pole parameters for describing the unit cell is found from a FEM program based on the conditions specified in Eq. (12). The reverberation time *RT* in the receiving room is assumed as 1 s. The sound pressure level difference D between rooms is corrected by $10\log(RT / 0.16V_{r2}) = -8\,\text{dB}$ to obtain the SRI according to Eq. (18).

Similar to Sec. 3.1, a FEM model is built for comparison, whose mesh is generated based on 300 Hz wavelength. In Fig. 12 (a) & (b), the spatial averaged SPL in the source and receiving room, predicted using the proposed approach and FEM, are compared below 500 Hz. The resultant SRI is compared in Fig. 13 (a). Again, the curves from the proposed approach and FEM agree perfectly before the FEM convergence limit, whereas slight discrepancies occur from 300 Hz to 500 Hz. The accuracy of the proposed approach is thus verified. In terms of calculation time, the

FEM model takes 4.5 days to solve 5×10^5 DOFs, while the sub-structuring model only takes 2 hours, both performed on the same workstation. The huge difference in the CPU time highlights the advantage of the proposed approach in the calculation efficiency.

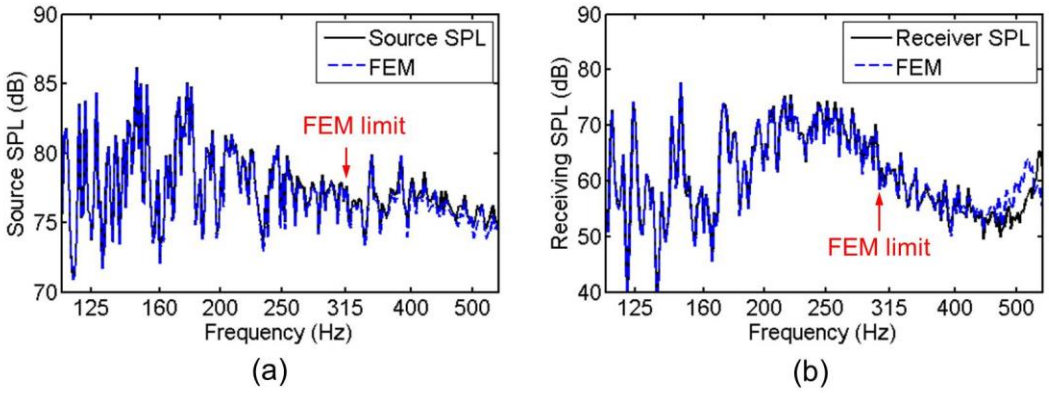

Fig. 12. The spatial averaged SPL in the: (a) source room; (b) receiving room, predicted using the proposed sub-structuring approach and FEM.

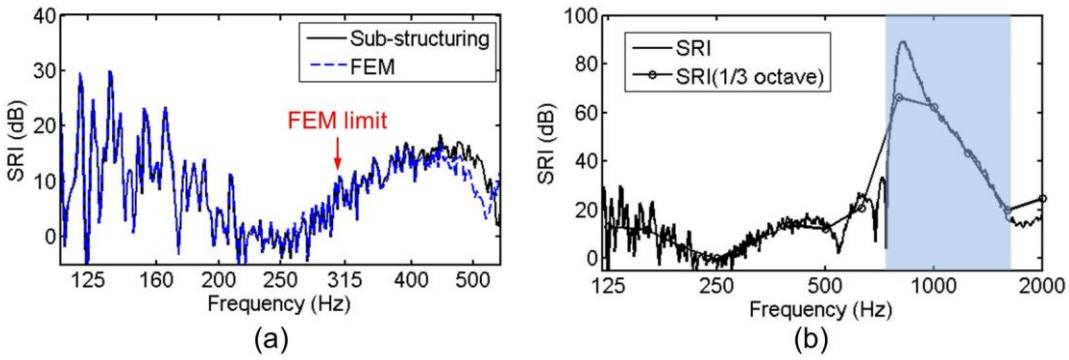

Fig. 13. SRI of the AMS in Fig. 9: (a) prediction using the proposed approach and FEM below 500 Hz; (b) prediction using the proposed approach up to 2000 Hz and 1/3 octave band SRI.

Figure 13(b) further presents the SRI of the AMS in the frequency range from 125 Hz to 2000 Hz, predicted using the proposed approach. It can be seen that strong

sound attenuation over 30 dB occurs from 600 Hz to 1600 Hz, coincides with the acoustic stop-band in the unit cell study. This range can be potentially used to tackle traffic noise ingress into the building. For example, building façade or window made of the present AMS structure can potentially satisfy the noise mitigation, natural ventilation and lighting requirements together. The proposed AMS structure, with a total thickness of l=0.1 m, can provide broadband control of sound waves whose frequencies are in the range of $0.2c_0/l$ to $0.5c_0/l$.

3.3 Other unit cell configurations

For comparison, two more cases with unit cell made of other acoustic elements are studied. As shown in Fig. 14(a), a straight air duct is considered in a unit cell with the the same dimension as the above case. The straight duct has a cross-section of 0.06×0.06 m and a length of l=0.1 m, with all the other part of the unit cell being assumed as rigid. The cut-off frequency of the duct is around 3000 Hz, which means that only plane wave can propagate in it below 2000 Hz. This allows the four-pole parameter to be derived analytically as:

$$\begin{bmatrix} P_1 \\ V_1 \end{bmatrix} = \begin{bmatrix} A & B \\ C & D \end{bmatrix} \begin{bmatrix} P_2 \\ V_2 \end{bmatrix} = \begin{bmatrix} \cos(kl) & j\sin(kl)\rho_0 c_0 \\ j\sin(kl)/\rho_0 c_0 & \cos(kl) \end{bmatrix} \begin{bmatrix} P_2 \\ V_2 \end{bmatrix}. \quad (21)$$

where l is the length of the straight duct. In another case, Fig. 14(b), the unit cell is changed to a simple expansion chamber. The unit cell dimension and the opening size are kept as the same. Since the interested frequency exceeds the cut-off frequency of the chamber, FEM model is used to derive the four-pole parameters, which takes into account the higher-order modes effect.

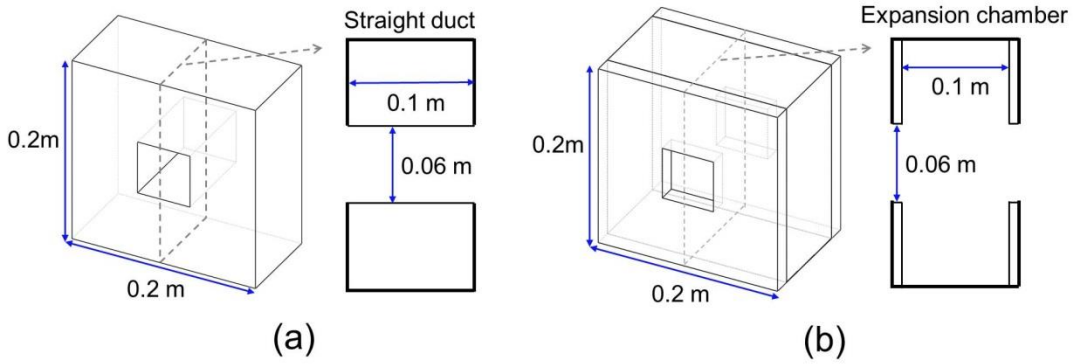

Fig. 14. (a) Unit cell with a straight air duct in the center; (b) Unit cell in the shape of an expansion chamber.

In Figs. 15 (a) and (b), the SRI results predicted using the proposed sub-structuring approach for the above two cases are presented. Note that validation against full FEM calculation below 300 Hz, similar to Figs. 8 and 12, has been checked (not shown here) and excellent agreements were observed. For the straight duct case in Fig. 14(a), it can be seen that the 1/3 octave band SRI is typically low, in the range of 10 ~ 15 dB, and shows dome-like behavior. The attenuation can be explained by the area change between the aperture and the unit cell, causing part of the incident energy to reflect back. The attenuation peak and dip appeared at around 650 Hz and 1300 Hz is due to the duct axial mode, where the wavelength is a quarter and half of the duct length. $f_{peak} = c_0 / 4L_{eff}$ and $f_{dip} = c_0 / 2L_{eff}$, respectively. The effective duct length can be estimated by $L_{eff} = l + 0.5h$, where h is the height of the unit cell opening [28]. As for the expansion chamber case in Fig. 15(b), the SRI shows a broad attenuation effect from 500 Hz to 2000 Hz. Since the aspect ratio of the expansion chamber (l/H, l=0.1 m, H is the chamber height H=0.2 m) is small, the repeating dome behavior in the

transmission loss disappears since the length of the resonator is not sufficient for the higher-order modes to decay. The unit cell therefore behaves like a cavity resonator [34].

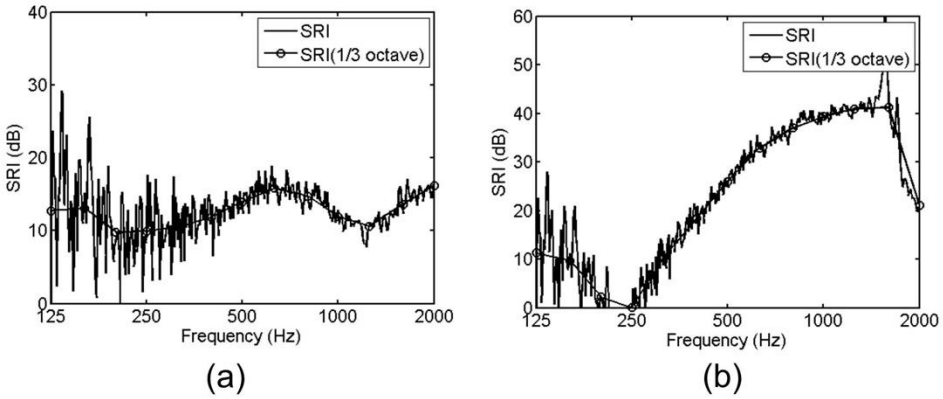

Fig. 15. SRI of an array of unit cells in (a) Fig. 14(a) (straight duct); (b) Fig. 14(b) (expansion chambers).

The SRI responses of the three cases as investigated above are summarized and compared in Fig. 16. It can be seen that the AMS provides the strongest attenuation near 1000 Hz, owing to the stop-band property of the unit cell. The straight duct unit cell shows relatively flattened behavior, with SRI mainly determined by the ratio between the aperture area and the total surface area. The acoustically short expansion chamber shows a more broadband sound insulation. It can be anticipated that the geometry, inner structure of a unit cell can be further tuned to suit particular applications with specific frequency signatures, where the proposed approach can be employed as an efficient design and optimization tool.

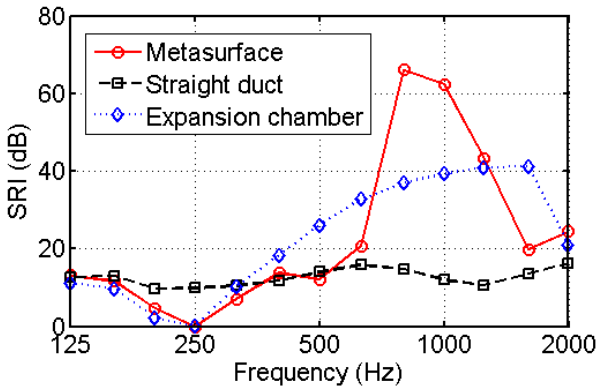

Fig. 16. Comparison of the resultant SRI with different unit cell configurations.

4. Conclusions

This paper presents a theoretical investigation on the sound insulation of acoustic metasurface, which is constructed of tailored acoustic unit cells in a planar array. The sound insulation was studied in a standard configuration, where acoustic excitation was generated by a diffuse sound source, and sound radiation into a receiving room was evaluated. A hybrid theoretical-numerical approach capable of handling acoustic predictions in the frequency range from 125 Hz to 2000 Hz has been developed. The modeling was deterministic, sub-structure based. The unit cells constituting the AMS were modeled using FEM to cope with complex geometries, which were assembled together to describe the surface property. The acoustic fields in the adjacent rooms were expressed in terms of the normal acoustic modes to save the computational cost. To facilitate the coupling treatment, subsystems were assembled based on their transfer function relationships at the interfaces, where the pressure and the velocity conditions were matched over small surface elements called "*patches*". The

computational cost was shown to be significantly reduced by enabling hybrid modeling methods for the AMS and the adjacent acoustic domains.

One of the aims of this study was to investigate the feasibility of developing AMS with both sound attenuation and ventilation ability. The unit cell configuration in the form of a waveguide loaded with periodic resonators, also forming an air ventilation path, was considered. Theoretical analysis based on the unit cell first revealed the existence of acoustic stop-band in the periodic structure, mainly due to accumulated scatterer resonance effect. The sound insulation for the AMS was then evaluated, showing remarkable attenuation performance can be achieved in the stop-band frequency range. The study could lead to interesting applications such as novel building façade and acoustic enclosure for practical noise control. The attenuation band could be controlled by a number of factors, e.g., the configuration and geometry of the unit cell, resonance and dissipation of the connected resonator, periodicity, arrangement of AMS, etc. The proposed approach could potentially address the need for better acoustic design and optimization.

The advantages are briefly summarized. First, the sub-structure framework allows using hybrid numerical methods to model a system. Significantly less CPU time has been demonstrated, which could play a vital role in future optimization study. Secondly, the method by which the SRI was evaluated was standard, making it possible to conduct comparisons between different designs and experimental results. Lastly, the proposed AMS treatment could lend itself to a wide range of extensions from the present configurations, where the unit cells were simply kept as the same.

For example, unit cells having different phase response can be constructed to realize wave front modulation [10], or locally resonant membranes can be combined to achieve deep subwavelength sound control [9]. The presented numerical tool provides a flexible tool to study the acoustic performance of these configurations.

Acknowledgements

This material is based on research/work supported by the Singapore Ministry of National Development and National Research Foundation under L2 NIC award No. L2NICCFP1-2013-9.

REFERENCES

[1] H.V. Fuchs, X. Zha, X. Zhou, H. Drotleff, Creating low-noise environments in communication rooms, Applied Acoustics, 62 (2001) 1375-1396.

[2] X. Yu, S.-K. Lau, L. Cheng, F. Cui, A numerical investigation on the sound insulation of ventilation windows, Applied Acoustics, 117, Part A (2017) 113-121.

[3] Z. Liu, X. Zhang, Y. Mao, Y.Y. Zhu, Z. Yang, C.T. Chan, P. Sheng, Locally Resonant Sonic Materials, Science, 289 (2000) 1734-1736.

[4] G. Ma, P. Sheng, Acoustic metamaterials: From local resonances to broad

horizons, Science Advances, 2 (2016).

[5] N. Fang, D. Xi, J. Xu, M. Ambati, W. Srituravanich, C. Sun, X. Zhang, Ultrasonic metamaterials with negative modulus, Nat Mater, 5 (2006) 452-456.

[6] S.H. Lee, C.M. Park, Y.M. Seo, Z.G. Wang, C.K. Kim, Composite Acoustic Medium with Simultaneously Negative Density and Modulus, Physical Review Letters, 104 (2010) 054301.

[7] K.J.B. Lee, M.K. Jung, S.H. Lee, Highly tunable acoustic metamaterials based on a resonant tubular array, Physical Review B, 86 (2012) 184302.

[8] Y. Cheng, C. Zhou, B.G. Yuan, D.J. Wu, Q. Wei, X.J. Liu, Ultra-sparse metasurface for high reflection of low-frequency sound based on artificial Mie resonances, Nat Mater, 14 (2015) 1013-1019.

[9] G. Ma, M. Yang, S. Xiao, Z. Yang, P. Sheng, Acoustic metasurface with hybrid resonances, Nat Mater, 13 (2014) 873-878.

[10] Y. Xie, W. Wang, H. Chen, A. Konneker, B.-I. Popa, S.A. Cummer, Wavefront modulation and subwavelength diffractive acoustics with an acoustic metasurface, Nat Commun, 5 (2014).

[11] C. Yang, L. Cheng, Sound absorption of microperforated panels inside compact acoustic enclosures, Journal of Sound and Vibration, 360 (2016) 140-155.

[12] ISO, 10140 Acoustics, Laboratory measurement of sound insulation of building elements.

[13] J. Poblet-Puig, A. Rodríguez-Ferran, Modal-based prediction of sound transmission through slits and openings between rooms, Journal of Sound and

Vibration, 332 (2013) 1265-1287.

[14] X. Yu, F.S. Cui, L. Cheng, On the acoustic analysis and optimization of ducted ventilation systems using a sub-structuring approach, The Journal of the Acoustical Society of America, 139 (2016) 279-289.

[15] X. Yu, L. Cheng, J.-L. Guyader, On the modeling of sound transmission through a mixed separation of flexible structure with an aperture, The Journal of the Acoustical Society of America, 135 (2014) 2785-2796.

[16] J. Pan, C.H. Hansen, D.A. Bies, Active control of noise transmission through a panel into a cavity: I. Analytical study, The Journal of the Acoustical Society of America, 87 (1990) 2098-2108.

[17] R. Panneton, N. Atalla, Numerical prediction of sound transmission through finite multilayer systems with poroelastic materials, The Journal of the Acoustical Society of America, 100 (1996) 346-354.

[18] G. Veronesi, E.J.M. Nijman, On the sampling criterion for structural radiation in fluid, The Journal of the Acoustical Society of America, 139 (2016) 2982-2991.

[19] B. van der Aa, J. Forssén, Scattering by an array of perforated cylinders with a porous core, The Journal of the Acoustical Society of America, 136 (2014) 2370-2380.

[20] V. Fokin, M. Ambati, C. Sun, X. Zhang, Method for retrieving effective properties of locally resonant acoustic metamaterials, Physical Review B, 76 (2007).

[21] N. Sui, X. Yan, T.-Y. Huang, J. Xu, F.-G. Yuan, Y. Jing, A lightweight yet sound-proof honeycomb acoustic metamaterial, Applied Physics Letters, 106 (2015) 171905.

[22] S. Varanasi, J.S. Bolton, T.H. Siegmund, R.J. Cipra, The low frequency performance of metamaterial barriers based on cellular structures, Applied Acoustics, 74 (2013) 485-495.

[23] C.J. Naify, C.-M. Chang, G. McKnight, S.R. Nutt, Scaling of membrane-type locally resonant acoustic metamaterial arrays, The Journal of the Acoustical Society of America, 132 (2012) 2784-2792.

[24] C.E. Bradley, Time harmonic acoustic Bloch wave propagation in periodic waveguides. Part I. Theory, The Journal of the Acoustical Society of America, 96 (1994) 1844-1853.

[25] C.E. Bradley, Time harmonic acoustic Bloch wave propagation in periodic waveguides. Part II. Experiment, The Journal of the Acoustical Society of America, 96 (1994) 1854-1862.

[26] V.M. García-Chocano, R. Graciá-Salgado, D. Torrent, F. Cervera, J. Sánchez-Dehesa, Quasi-two-dimensional acoustic metamaterial with negative bulk modulus, Physical Review B, 85 (2012) 184102.

[27] M.-C. Chiu, Y.-C. Chang, Shape optimization of multi-chamber cross-flow mufflers by SA optimization, Journal of Sound and Vibration, 312 (2008) 526-550.

[28] X. Yu, L. Cheng, Duct noise attenuation using reactive silencer with various internal configurations, Journal of Sound and Vibration, 335 (2015) 229-244.

[29] T.W. Wu, P. Zhang, C.Y.R. Cheng, BOUNDARY ELEMENT ANALYSIS OF MUFFLERS WITH AN IMPROVED METHOD FOR DERIVING THE FOUR-POLE PARAMETERS, Journal of Sound and Vibration, 217 (1998) 767-779.

[30] R. Kirby, A comparison between analytic and numerical methods for modelling automotive dissipative silencers with mean flow, Journal of Sound and Vibration, 325 (2009) 565-582.

[31] S.-H. Seo, Y.-H. Kim, Silencer design by using array resonators for low-frequency band noise reduction, The Journal of the Acoustical Society of America, 118 (2005) 2332-2338.

[32] C.I. Papadopoulos, Development of an optimised, standard-compliant procedure to calculate sound transmission loss: design of transmission rooms, Applied Acoustics, 63 (2002) 1003-1029.

[33] H. Nélisse, J. Nicolas, Characterization of a diffuse field in a reverberant room, The Journal of the Acoustical Society of America, 101 (1997) 3517-3524.

[34] A. Selamet, P. Radavich, The effect of length on the acoustic attenuation performance of concentric expansion chambers: an analytical, computational and experimental investigation, Journal of Sound and Vibration, 201 (1997) 407-426.

Table Caption

Table 1. The number of acoustic modes N_m within the frequency range from 0 to the upper limit of each 1/3 octave band.

Figure Captions

Fig. 1. (a) AMS constructed of structured unit cells for controlling and manipulating sound waves; (b) AMS connecting a sound source field and a receiving room.

Fig. 2. Sub-structuring approach for modeling the sound transmission between two rooms through the AMS.

Fig. 3. Modeling of the AMS mounted on the common partition wall.

Fig. 4. AMS modeled as: (a) an equivalent acoustic domain; (b) an array of acoustic elements. (c) AMS with unit cells designed in an air duct with periodic resonators.

Fig. 5. A representative source room to excite the test AMS structure.

Fig. 6. Standard deviation of SPLs in the sampled region in the source room.

Fig. 7. Configuration and dimensions of the source room, reciving room and opening.

Fig. 8. Comparisons between the SPLs calculated using the proposed approach and FEM, at: (a) P1 in the source room and (b) P2 in the receiving room.

Fig. 9. (a) Acoustic metasurface constructed from a planar array (5×5) of unit cells; (b) 3D configuration of a unit cell, consisting of a serious of expansion chambers; (c) Inner dimension of the 2D cross-section.

Fig. 10. (a) The fabricated unit cell sample for experimental test. (b) FEM model for calculating the transmission characteristics of a unit cell.

Fig. 11. (a) The transmittance versus frequency, the bandgap structure is marked in light blue. (b) Transmission loss of the unit cell.

Fig. 12. The spatial averaged SPL in the: (a) source room; (b) receiving room, predicted using the proposed sub-structuring approach and FEM.

Fig. 13. SRI of the AMS in Fig. 9: (a) prediction using the proposed approach and FEM below 500 Hz; (b) prediction using the proposed approach up to 2000 Hz and 1/3 octave band SRI.

Fig. 14. (a) Unit cell with a straight air duct in the center; (b) Unit cell in the shape of an expansion chamber.

Fig. 15. SRI of an array of unit cells in (a) Fig. 14(a) (straight duct); (b) Fig. 14(b) (expansion chambers).

Fig. 16. Comparison of the resultant SRI with different unit cell configurations.